Agricultural and Forest Meteorology 253–254 (2018) 84–93

Contents lists available at ScienceDirect

Agricultural and Forest Meteorology

journal homepage: www.elsevier.com/locate/agrformet

A new estimation of China's net ecosystem productivity based on eddy covariance measurements and a model tree ensemble approach

Yitong Yao[a,1], Zhijian Li[b,1], Tao Wang[c,d,*], Anping Chen[e], Xuhui Wang[a,f], Mingyuan Du[g], Gensuo Jia[h], Yingnian Li[i], Hongqin Li[i], Weijun Luo[j,k], Yaoming Ma[c,d], Yanhong Tang[l], Huimin Wang[m], Zhixiang Wu[n], Junhua Yan[o], Xianzhou Zhang[m], Yiping Zhang[p], Yu Zhang[q], Guangsheng Zhou[r], Shilong Piao[a,c,d]

[a] Sino-French Institute for Earth System Science, College of Urban and Environmental Sciences, Peking University, Beijing 100871, China
[b] Zhan Jiang Urban Planning Bureau, Zhanjiang 524022, China
[c] Key Laboratory of Alpine Ecology and Biodiversity, Institute of Tibetan Plateau Research, Chinese Academy of Sciences, Beijing 100085, China
[d] Center for Excellence in Tibetan Earth Science, Chinese Academy of Sciences, Beijing 100085, China
[e] The Woods Hole Research Center, Falmouth, MA 02540, USA
[f] Laboratoire de Météorologie Dynamique, Institute Pierre-Simon Laplace, 95005 Paris, France
[g] Institute for Agro-Environmental Sciences, National Agriculture and Food Research Organization, Tsukuba 305-8604, Japan
[h] CAS Key Laboratory of Regional Climate-Environment for Temperate East Asia, Institute of Atmospheric Physics, Chinese Academy of Sciences, Beijing 100029, China
[i] Key Laboratory of Adaptation and Evolution of Plateau Biota, Northwest Institute of Plateau Biology, Chinese Academy of Sciences, Xining 810008, China
[j] State Key Laboratory of Environmental Geochemistry, Institute of Geochemistry, Chinese Academy of Sciences, Guiyang 550081, China
[k] Puding Karst Ecosystem Research Station, Chinese Academy of Sciences, Puding 562100, China
[l] Department of Ecology, College of Urban and Environmental Sciences, Peking University, Beijing 100871, China
[m] Key Laboratory of Ecosystem Network Observation and Modeling, Institute of Geographic Sciences and Natural Resources Research, Chinese Academy of Sciences, Beijing 100101, China
[n] Rubber Research Institute, Chinese Academy of Tropical Agricultural Sciences, Danzhou 571737, China
[o] South China Botanical Garden, Chinese Academy of Sciences, Guangzhou 510650, China
[p] Key Laboratory of Tropical Forest Ecology, Xishuangbanna Tropical Botanical Garden, Chinese Academy of Sciences, Mengla, Yunnan 666303, China
[q] Cold and Arid Regions Environmental and Engineering Research Institute, Chinese Academy of Sciences, Lanzhou 730000, China
[r] State Key Laboratory of Vegetation and Environmental Change, Institute of Botany, Chinese Academy of Sciences, Beijing 100093, China

ARTICLE INFO

Keywords:
Net ecosystem productivity (NEP)
Model tree ensemble
China
Eddy covariance
Carbon sink

ABSTRACT

Accurate assessment of the strength of China's terrestrial ecosystem carbon sink is key to understanding its regional carbon budget. However, large uncertainties in current carbon sink estimations still exist, which hinder the prediction of future climate change trajectories. In this study, we generated a high-resolution (1 km × 1 km) dataset of China's net ecosystem productivity (NEP) in the last decade via a model tree ensemble approach combined with data from 46 flux sites in China and neighboring regions. The upscaling also included detailed information on nitrogen (N) deposition and forest age that have often been neglected in previous studies. The performance of MTE algorithm in simulating NEP at the site level is relatively high for both training (R^2 = 0.81, RMSE = 0.73 gC m^{-2} day^{-1}) and validation datasets (R^2 = 0.76, RMSE = 0.81 gC m^{-2} day^{-1}). Our data-driven estimation showed that roughly 70% of the area is a carbon sink, and the largest carbon sinks are found in the southeast and southwest monsoon regions. The total annual NEP in China in the last decade was 1.18 ± 0.05 Pg C yr^{-1}, which is similar to the results found by another foundational global-scale study. Yet, the two studies significantly differ in the spatial distribution of carbon sink density. The seasonality of China's NEP is characterized by region-specific kurtosis and skewness in most areas. Furthermore, ecosystem carbon use efficiency (CUE), defined as the annual NEP/GPP ratio, also showed high spatial variation. For example, the Xiaoxing'anling and Changbai Mountains in northeastern China, the eastern edge of the Tibetan Plateau, and bordering areas of the southeast and southwest monsoon regions have a larger CUE than the rest of China. On average, China's terrestrial ecosystem CUE is approximately 0.17. Our data-driven NEP and CUE estimates

* Corresponding author at: Key Laboratory of Alpine Ecology and Biodiversity, Institute of Tibetan Plateau Research, Chinese Academy of Sciences, Beijing 100085, China.
E-mail address: twang@itpcas.ac.cn (T. Wang).
[1] Both authors contributed equally to this work.

https://doi.org/10.1016/j.agrformet.2018.02.007
Received 5 August 2017; Received in revised form 5 February 2018; Accepted 8 February 2018
Available online 17 February 2018
0168-1923/ © 2018 Elsevier B.V. All rights reserved.

provide a new tool for assessing China's carbon dioxide flux. Our study also highlights the necessity to incorporate more environmental variables related to vegetation growth and more data derived from flux sites into NEP upscaling to reduce uncertainties in carbon budget estimations.

1. Introduction

Increasing atmospheric carbon dioxide (CO_2) concentrations, mainly caused by anthropogenic activities, including fossil fuel burning and deforestation, have been altering the Earth's systems and threatening human survival (Intergovernmental Panel on Climate Change [IPCC], 2013). As a large carbon (C) sink, terrestrial ecosystems annually sequester about 3 Pg C from the atmosphere, which accounts for 30% of anthropogenic emitted CO_2 in the last decade (Le Quéré et al., 2015). Terrestrial C sinks, however, have large spatial and temporal variability (Gurney and Eckels, 2011; Le Quéré et al., 2009; Luyssaert et al., 2008; Pan et al., 2011; Piao et al., 2009a; Wang et al., 2014). Monitoring and understanding the spatiotemporal variation in terrestrial C balance is a key step in accurately predicting future climate change scenarios (Friedlingstein et al., 2006, 2014; Gregory et al., 2009) and developing climate negotiations strategies. Thus, the IPCC (2013) has recognized it as an important global issue.

During the last four decades, several approaches have been developed to quantify C sequestration in terrestrial ecosystems at the regional and global scales including atmospheric inversions (Denning et al., 1996; Tans et al., 1990), process-based ecosystem models (Krinner et al., 2005; Sitch et al., 2003), inventory approaches (Pacala et al., 2001; Pan et al., 2011), and eddy covariance (EC) flux data oriented regional or global estimations of C flux (Jung et al., 2011; Xiao et al., 2008, 2011a). Among these approaches, EC flux data oriented regional estimations of Net Ecosystem Productivity (NEP) has been widely used to understand spatiotemporal patterns of C balance and its controlling processes (Schwalm et al., 2012; Xiao et al., 2011b). This method has even been applied to evaluate process-based ecosystem models as 'observations' (Anav et al., 2013; Piao et al., 2013). It should be noted that only variables indicating vegetative characteristics (e.g., the fraction of absorbed photosynthetic active radiation [FPAR] derived from remote sensing and land cover) and climate have been taken into account when upscaling CO_2 fluxes from flux networks to the regional or global scale in previous studies (Jung et al., 2011; Xiao et al., 2008, 2011a). However, other factors such as forest stand age and nitrogen (N) deposition can similarly help determine the C exchange between terrestrial systems and the atmosphere by regulating gross primary productivity (GPP) and terrestrial ecosystem respiration (TER) (Hyvönen et al., 2007). For example, there is a general consensus that NEP increases with stand age in young forests but declines in old forests (Goulden et al., 2011; Luyssaert et al., 2008). It has also been suggested that N deposition enhances NEP through increasing GPP and declining soil respiration, although the magnitude of the effect of N deposition on NEP remains poorly quantified (De Vries et al., 2009; Magnani et al., 2007; Sutton et al., 2008). These findings highlight the necessity of integrating stand age and N deposition into approaches that upscale FLUXNET observations of CO_2 to regional or global scale estimations of NEP.

China has the most diverse climate regimes and ecosystems in the world. Thus, knowledge of its C sources and sinks, their spatial distributions, and the underlying mechanisms can improve the understanding of global C cycles (Canadell et al., 2011). To this end, since the early 2000s, great efforts have been made to investigate the magnitude and distribution of C sinks and sources in China (Cao et al., 2003; Fang et al., 2007; Piao et al., 2009b; Tian et al., 2011a, 2011b; Yu et al., 2014), but studies significantly differ regarding the magnitude of China's C budget (Cao et al., 2003; Piao et al., 2009b). This is partly due to the lack of direct *in situ* observations of NEP. To overcome this limitation, China has built more than 100 EC flux towers in a variety of ecosystems during the past 10 years (Yu et al., 2006a, 2006b, 2016). In this study, we upscaled China's FLUXNET observations of NEP to the country scale using a machine-learning technique (model tree ensemble, MTE) (Jung et al., 2009, 2011). The MTE algorithm used in this study is notable for its step-wise regression mode in leaf nodes rather than constant number like Regression Tree, its ensemble attributes and its processing capacity on categorical variables that are all superior to most of machines learning methods (Jung et al., 2009). Note that due to the lack of data sharing, only 46 flux sites in (37 sites) and near (9 sites) China are used in this study, but this is far more than the number of Chinese sites (only 9) used in determining global NEP in a previous foundational study (Jung et al., 2011). Moreover, in addition to satellite-observed FPAR, vegetation distribution, and climate variables, both forest stand age and N deposition are also taken into account in our MTE approach.

Since including much more flux sites in the Asian region and taking

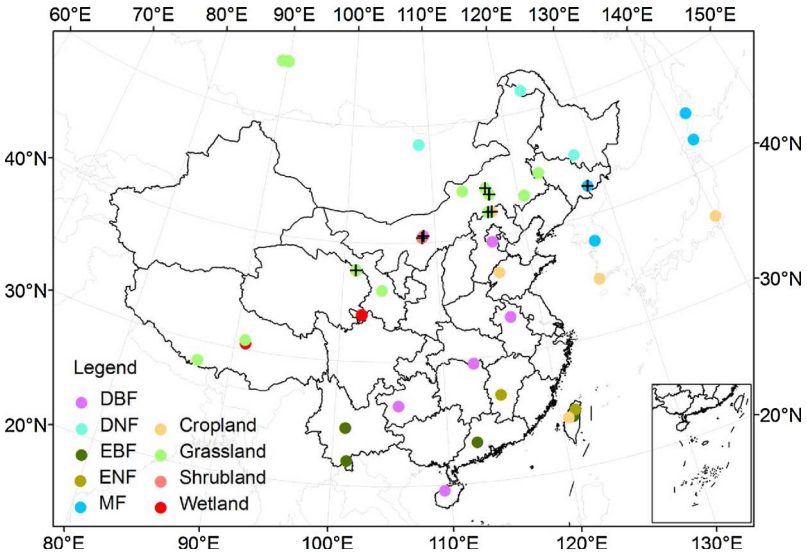

Fig. 1. The spatial distribution of eddy covariance flux towers used in our model tree ensemble approach (n = 46). The 9 flux sites used in Jung et al. (2011) are displayed as colored circle with a black cross. DBF: deciduous broadleaf forest, DNF: deciduous needleleaf forest, EBF: evergreen broadleaf forest, ENF: evergreen needleleaf forest, MF: needleleaf and broadleaf mixed forest.

into account the effects of forest age and N deposition would significantly improve the estimation of Chinese NEP, here we compared our estimate to the previous global estimate by Jung et al. (2011) in terms of spatial variation, seasonal distribution, and ecosystem carbon use efficiency (CUE).

2. Material and methods

2.1. Collection of EC flux data

EC technique has been widely used for the direct measurement of net C exchange between atmospheric and terrestrial ecosystems (Baldocchi, 2008, 2014). EC flux towers provide half-hourly values of net CO_2 exchange with positive values indicating the C lost to the atmosphere and negative values indicating the net gain of C by the ecosystems. Net ecosystem exchange (NEE) with a change in sign is often referred to as approximate Net Ecosystem Productivity (NEP = −NEE). We collected flux data from ChinaFlux (www.chinaflux.org) (Yu et al., 2006b), AsiaFlux (www.asiaflux.net) (Saigusa et al., 2013), and the global FLUXNET database (www.fluxdata.org) (Baldocchi, 2008). In total, 46 sites were included in this study (Fig. 1 and Table A.1 in the Supplementary material), encompassing nine typical vegetation types in China: deciduous broadleaf forest (DBF), deciduous needleleaf forest (DNF), evergreen broadleaf forest (EBF), evergreen needleleaf forest (ENF), mixed forest (MF), cropland, grassland, shrubland, and wetland. The original flux data in half-hour frequencies were first aggregated to daily values and averaged within 1 month. These collected flux data span from 2001 to 2015. Totally 1181 site-month flux data points were used for construction of the Chinese NEP dataset after quality control.

2.2. Climate and satellite input datasets

Monthly air temperature, total precipitation, and shortwave radiation used in this study were obtained from a dataset developed by the hydro-meteorological research group at the Institute of Tibetan Plateau Research, Chinese Academy of Sciences (Chen et al., 2011; Yang et al., 2010). The temporal and spatial resolutions of these climate datasets used a daily frequency of 0.1° × 0.1°, respectively. Temperature data were obtained by merging China Meteorological Administration (CMA) observations into the Princeton meteorological forcing data (Sheffield et al., 2006). Precipitation data were a combination of Tropical Rainfall Measuring Mission data products (Huffman et al., 2007), CMA operational observation stations, and Asian Precipitation–High Resolution Observational Data Integration Toward Evaluation of Water Resources data (Yatagai et al., 2009). Shortwave radiation data were obtained by incorporating available CMA radiation observations with the correct Global Energy and Water Cycle Experiment–Surface Radiation Budget and a hybrid radiation model (Yang et al., 2006). This reanalysis dataset was evaluated against quality-checked shortwave radiation data at 95 CMA stations and other independent datasets such as data from the Coordinated Enhanced Observing Period Asia-Australia Monsoon Project-Tibet (Chen et al., 2011). In this study, the daily data were arithmetically averaged, maximized, or summed to provide monthly values. We used monthly mean temperature, monthly maximum temperature, monthly total precipitation, and monthly mean radiation as explanatory variables in NEP upscaling.

The FPAR is a biophysical indicator that reflects the vegetation canopy energy absorption capacity (Myneni et al., 2002). A Moderate Resolution Imaging Spectroradiometer onboard the Terra satellite has provided global FPAR data products (MOD15A2) in 1 km × 1 km spatial resolution and 8-day time intervals since 2000. These data were downloaded from https://lpdaac.usgs.gov/data_access/data_pool. The original 8-day FPAR data were first aggregated to monthly intervals using a maximum value composition approach (Holben, 1986). Monthly FPAR was also used as an explanatory variable in NEP upscaling.

2.3. Forest age dataset

Forest stand age is a meaningful metric in reflecting ecosystem disturbance history and quantifying C sequestration potential (Gao et al., 2016; Pregitzer and Euskirchen, 2004; Yu et al., 2014; Zhang et al., 2017). To incorporate forest age effects into our forest NEP estimations, we applied a Chinese forest age map developed by Zhang et al. (2017). This Chinese forest age map, which uses 2005 as a reference year, was generated in a 1 km × 1 km spatial resolution by downscaling the provincial statistics from national forest inventory data in combination with climate data and tree height data (Fig. A.1 in the Supplementary material). In this study, forest age was used as an explanatory variable in forest NEP upscaling.

2.4. N deposition dataset

We used the N deposition dataset from the Multi-scale Synthesis and Terrestrial Model Inter-comparison Project environmental forcing data (Wei et al., 2014), which was generated via interpolating the Dentener global N deposition data product in 1860, 1993, and 2050 (Dentener, 2006) using an approach described in Tian et al. (2010) and Lu et al. (2012). These dataset encompassed spatial and temporal N emission variation, and provided time-varying annual N deposition rates (NHx-N and NOy-N) at 0.5° × 0.5° resolution from 1860 to 2050. Then we were able to extract corresponding annual N deposition rates for each flux measurement. We resampled the N deposition data to 1 km × 1 km resolution using the nearest neighbor method. The mean annual N deposition rate during 2005–2015 is shown in Fig. A.2 in the Supplementary material. The annual N deposition rate was also used as an explanatory variable in NEP upscaling.

2.5. Chinese vegetation distribution map

In this study, we used the 1:1000,000 Chinese vegetation distribution map (Editorial Board of Vegetation Map of China, 2007). The original 573 types were first reclassified into nine vegetation types including DBF, DNF, EBF, ENF, MF, cropland, grassland, shrubland, and wetland, which are the same as the 9 typical vegetation types at the flux sites.

We compared the Chinese vegetation map to the SYNMAP (reclassified into the IGBP classes) used in Jung et al. (2011). The SYNMAP does not include the wetland, but include needleleaf mixed forests and broadleaf mixed forests that are not considered in the Chinese vegetation map. So we mainly compare the distribution of the 8 vegetation types (DBF, DNF, EBF, ENF, MF, cropland, grassland and shrubland) (Fig. A.3 in the Supplementary material). Moreover, we also summarize the percent of consistency/inconsistency between the two vegetation maps in Table A.2 in the Supplementary material. In terms of cropland and grassland, the map consistency is higher than 50%. But the map consistency is only ~30% for the forest types such as DBF, EBF, ENF, and MF. There is notable regional difference between the two vegetation maps. For example, northern and northwestern parts of Tibetan Plateau are identified as grasslands in the Chinese vegetation map, but denoted as shrublands in SYNMAP. The border of Daxing'anling is classified as DNF in the Chinese vegetation map but as ENF for SYNMAP. In southern China, fraction of EBF in southwest area in SYNMAP is higher than that in the Chinese vegetation map. Shrubland mainly distributes around the Sichuan Basin from the Chinese vegetation map but much less shrubland is identified based on the SYNMAP.

2.6. Chinese NEP estimation

Here we applied a MTE approach to upscale the flux NEE measurement. The MTE method was first discussed by Jung et al. (2009) and has since been applied to upscale C and water flux at a global scale (Beer et al., 2010; Jung et al., 2010, 2011; Zeng et al., 2014). To avoid

the over-fitting, we firstly randomly divided the flux data into the two groups: 90% sample data (1063 site-months) as training dataset and the remaining 10% (118 site-months) as the validation dataset. The model trees were trained on site-level NEE using meteorological inputs, FPAR, vegetation type, forest age and N deposition based on the training dataset. The specific explanatory variables for NEP estimation are listed in Table A.3 in the Supplementary material, which are classified into two types: split & regression variables and split variables. The trained MTE is then applied on the validation dataset to test the MTE performance in NEE simulation. The output NEP estimation is the median of 25 independent best ensemble members. Finally, we obtained the time-varying NEP estimation in each pixel by applying the well-trained MTE on spatio-temporal varying gridded input datasets with 1km spatial resolution and monthly time step from the period 2005–2015.

2.7. Global NEP dataset

Jung et al. (2011) generated a 0.5° × 0.5° gridded monthly global NEP during 1982–2011 by training MTE over La Thuile NEE data with climatic factors (temperature, precipitation and potential radiation) and satellite-derived vegetation biophysical parameter (FPAR). We used the overlapped time span (2005–2011) of NEP in this study for their comparison.

2.8. Chinese GPP dataset

To calculate the CUE at ecosystem level, which is defined as the ratio between annual NEP and GPP (Fernández-Martínez et al., 2014), we employed the Chinese GPP dataset at 0.1° × 0.1° spatial resolution at monthly intervals (Yao et al., 2018). Applying the MTE method for both climate fields and satellite-based vegetation proxies generated this dataset. We subtracted the same time period of 2005–2015 from the Chinese GPP dataset and resampled it to 1 km × 1 km using the nearest neighbor method.

2.9. Comparison map profile method

To examine spatial similarity and different patterns between the annual NEP produced in this study and in Jung et al. (2011), we applied the comparison map profile (CMP) method, which is based on a similarity index computation (absolute distance [D] and cross-correlation coefficient [CC]) between moving windows of two spatially explicit datasets (Arnan et al., 2011; Gaucherel et al., 2008). The D between moving windows in the two compared NEP maps was calculated using Eq. (1), which provides an absolute value for the differences between them. A low D value indicates a good agreement between the moving windows.

$$D = \mathrm{abs}(\overline{x} - \overline{y}) \tag{1}$$

where $\overline{x}$ and $\overline{y}$ are the averaged NEP computed over two moving windows in two compared maps. The CC is calculated using Eq. (2), which suggests similar or contrasting directions in gradient (Gaucherel et al., 2010; Gritti et al., 2013). A low CC value indicates that the similarity between the two moving window in two maps is poor.

$$CC = \frac{1}{N^2}\sum_{i=1}^{N}\sum_{j=1}^{N}\frac{(x_{ij}-\overline{x}) \times (y_{ij}-\overline{y})}{\sigma_x \times \sigma_y} \tag{2}$$

$$\text{with } \sigma_x{}^2 = \frac{1}{N^2-1}\sum_{i=1}^{N}\sum_{j=1}^{N}(x_{ij}-\overline{x})^2 \tag{3}$$

where x_{ij} and y_{ij} are the pixel value at row i and column j of the two moving windows in the compared NEP maps. Each moving window covers N pixels. σ_x and σ_y are the standard deviations calculated within the two moving windows. By repeating these similarity index computations 20 times successively by increasing the window size from scale 1 (window size: 3 × 3 pixels) to scale 20 (window size: 41 × 41 pixels), maps of D and CC values are computed for each mono-scale. Calculations of scale 1 reflect an approximate pixel-to-pixel difference in the two maps, while scale 20 suggests a large gradient similarity or inconsistency between the two datasets. All of these mono-scale maps were combined into one mean CMP map by arithmetically averaging the similarity value over 20 mono-scales in each pixel. This method enables the quantification of differences both with regard to magnitude and the local gradient between the maps when changing spatial scales. The annual NEP produced in this study was resampled to a 0.5° × 0.5° resolution to match the NEP of Jung et al. (2011) during CMP comparison procedures. See Gaucherel et al. (2008) for detailed description of the CMP method.

2.10. Seasonal NEP statistics

Kurtosis is a descriptor of the shape of the probability distribution curve. Skewness is a measurement of the asymmetry of the probability distribution. Here we used kurtosis and skewness to characterize seasonal NEP in China. To transfer the multi-year averaged 12 monthly NEP values in each pixel to an equivalent distribution, we assumed 1000 numbers and repeated month i for instances of num_i. num_i was calculated using Eq. (4). Then we assembled all of these repeated months as array L (Eq. (5)). The length of array L was 1000. Finally, we obtained kurtosis and skewness of array L (Eqs. (6) and (7)). When individual monthly NEP was negative in one pixel, we added the reverse of the minimum value to all 12 monthly NEP values in that pixel.

$$num_i = \mathrm{round}\left(\frac{NEP_i}{\sum_{i=1}^{12} NEP_i} \times 1000\right)(i = 1,2,3,\ldots 11,12) \tag{4}$$

$$L = \{\overbrace{1,1,\ldots}^{num1}\overbrace{2,2,\ldots}^{num2}\ldots\ldots\overbrace{12,12,\ldots}^{num12}\} \tag{5}$$

where NEP_i is the mean monthly NEP value in month i and num_i is the repeated times for month i in array L.

$$\mathrm{kurtosis(L)} = \frac{\mu_4}{\sigma^4} = \frac{E[(L-\mu)^4]}{\sigma^4} - 3 \tag{6}$$

where μ_4 is the fourth central moment, μ is the mean, σ is the standard deviation, and E is the expectation operator.

$$\mathrm{skewness\ (L)} = \frac{\mu_3}{\sigma^3} = E\left[\frac{(L-\mu)^3}{\sigma}\right] \tag{7}$$

where μ_3 is the third central moment. Zero values for kurtosis and skewness correspond to a standard normal (gaussian) seasonal NEP distribution. A negative value for the skewness indicates a left-skewed data distribution and a peak value appearance suggests that it is skewed to later in the year. By contrast, positive skewness suggests a right-skewed seasonal dynamic. A negative kurtosis value represents a more leveled seasonal NEP distribution than normal and positive kurtosis reflects a sharp peak in seasonal cycles.

3. Results

3.1. MTE performance on estimating NEE

We used the R^2 coefficient and root mean square error (RMSE) to quantify the MTE algorithm performances on estimating NEE against observed NEE. The MTE estimated NEE showed great consistency with the flux observed NEE. Regarding the training samples, R^2 was 0.81 and RMSE was 0.73 $gC\,m^{-2}\,day^{-1}$ (Fig. 2), and similarly for validation samples, R^2 reached 0.76 and RMSE was 0.81 $gC\,m^{-2}\,day^{-1}$ (Fig. 2).

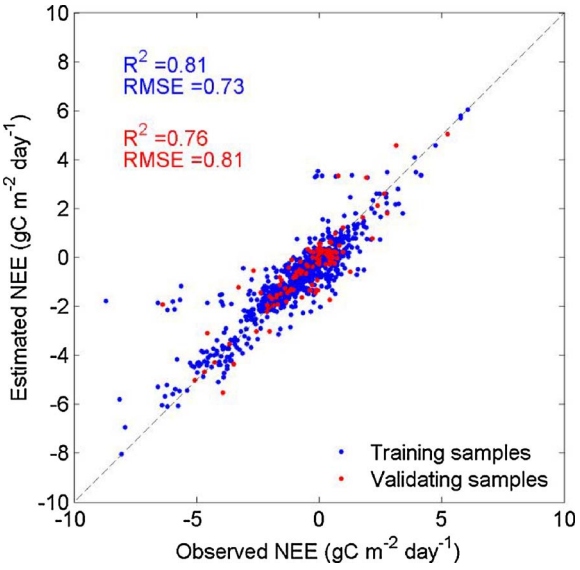

Fig. 2. The relationship between MTE predicted NEE and flux NEE observation. The performance of MTE is labeled.

3.2. Spatial distribution of mean annual Chinese NEP

Fig. 3a shows the spatial distribution of mean annual NEP during the period 2005–2011. A geological heterogeneity existed with a pronounced ascendant gradient. As shown in this figure, C sink density increased from northwest to southeast. The largest C sink mainly distributed in the two monsoon regions: southwest and southeast China, where the magnitude of the C sink was generally larger than 500 $gC\,m^{-2}\,yr^{-1}$. In addition to these two monsoon regions, mountainous regions such as Daxing'anling, Xiaoxing'anling, and the Changbai Mountains also had a relatively high C sink with a magnitude larger than 300 $gC\,m^{-2}\,yr^{-1}$. The North China Plain, Sichuan Basin, and central China generally had C sinks lower than 300 $gC\,m^{-2}\,yr^{-1}$. By contrast, terrestrial ecosystems in most of Inner Mongolia and the hinterland of the Tibetan Plateau acted as C source (Fig. 3a). Overall, our estimations suggest that about 70% of the area plays a role as C sink in China.

At the country scale, the annual NEP in China is about 1.18 ± 0.05 $Pg\,C\,yr^{-1}$ with C sink density of 158.9 $gC\,m^{-2}\,yr^{-1}$ from 2005 to 2015. This estimation is slightly lower (4.9%) than that of the study by Jung et al. (2011), who predicted that the magnitude of China's annual NEP was about 1.22 ± 0.06 $Pg\,C\,yr^{-1}$ during the same time period. Despite the similar magnitudes with regard to the total amount of C sinks in the two datasets, remarkably large discrepancies lie in their spatial distribution. For instance, compared to the estimation by Jung et al. (2011), our derived dataset estimated distinctly higher C sink density in the northeastern forested area of the country (Fig. 3a, b, more than 300 $gC\,m^{-2}\,yr^{-1}$ in this study versus less than 250 $gC\,m^{-2}\,yr^{-1}$ by Jung et al., 2011). By contrast, C sink density in the Sichuan Basin and in central China estimated in our study was dramatically lower than that from Jung et al. (2011) (Fig. 3a, b, less than 250 $gC\,m^{-2}\,yr^{-1}$ in our study versus greater than 300 $gC\,m^{-2}\,yr^{-1}$ by Jung et al., 2011). The percentage of area functioning as C sources in this study was higher than in Jung et al. (2011) (30.5% in this study versus 21.9% in Jung et al., 2011), and these additional C sources mainly distributed in the east of the Tibetan Plateau and part of the grassland areas in northeastern China.

Furthermore, we used the CMP method to explore the inconsistency of the spatial patterns of annual NEP estimations between our study and that by Jung et al. (2011). This approach included the comparison of spatial magnitudes and regional gradients of C sink density. Here, discrepancies of magnitudes and gradients were characterized by D and CC over spatial moving windows, respectively. Larger D and lower CC indicated more inconsistent magnitudes and local gradient distributions between the two datasets. The magnitude differences mainly existed around the Sichuan Basin, southwest China, and mountainous regions such as Daxing'anling, where the regional D between the two datasets exceeded 100 $gC\,m^{-2}\,yr^{-1}$ (Fig. A.4a in the Supplementary material). Regarding the spatial gradient comparison, the border of Daxing'anling had negative CC, which suggests a local reverse spatial gradient between the two datasets (Fig. A.4b in the Supplementary material). Furthermore, southern China also had an inconsistent spatial gradient, whose CC is below 0.2 (Fig. A.4b in the Supplementary material).

3.3. Seasonal cycles of NEP in China

The seasonal distribution of China's NEP is characterized by kurtosis and skewness (Fig. 4). Kurtosis is positive when the peak of the seasonal NEP is sharper than normal and vice versa. Spatially, the kurtosis values of China's seasonal NEP distribution range from –1.9 to 12.3, with the majority of areas having a negative kurtosis. This indicates that there is a more leveled seasonal NEP distribution than normal in most areas. The smallest kurtosis values were found in the southeast Tibetan Plateau and the southwest monsoon regions. However, in most areas of the Tibetan Plateau, the kurtosis value was positive (and the highest in China), suggesting an acute central NEP peak over a very short period (1–2 months). For the same region at the same period, our results of the kurtosis distributions of seasonal C sink density markedly differ from the findings of Jung et al. (2011). For instance, we found a lower kurtosis of seasonal NEP in the northeastern forested area, parts of North China, and the eastern edge of the Tibetan Plateau than did Jung et al. (2011) (Fig. 4a, c), meaning the duration of the large monthly local NEP was longer in our study than in Jung et al. (2011). By contrast, in Inner Mongolia and west of the Tibetan Plateau, the kurtosis values were more negative in Jung et al. (2011) than in our study (Fig. 4a, c).

Furthermore, we also used skewness to evaluate the asymmetry of

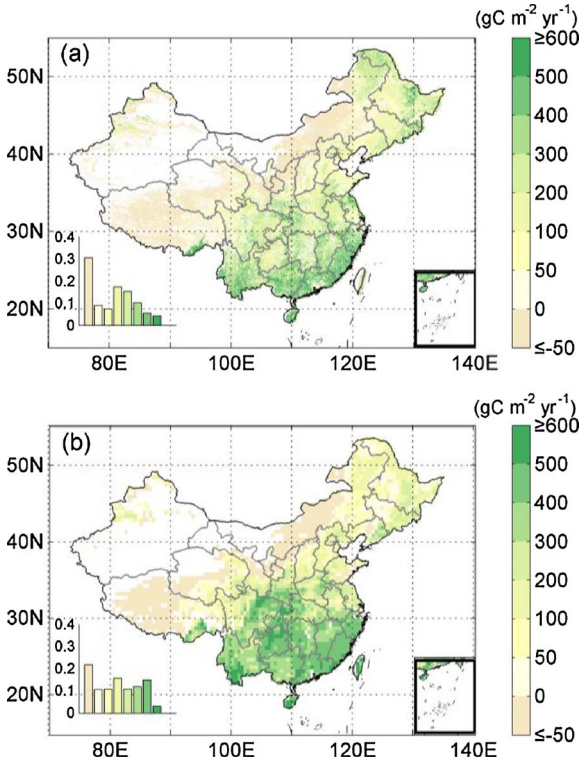

Fig. 3. The spatial pattern of the mean annual Chinese NEP from 2005 to 2011 from (a) our study and (b) Jung et al. (2011).

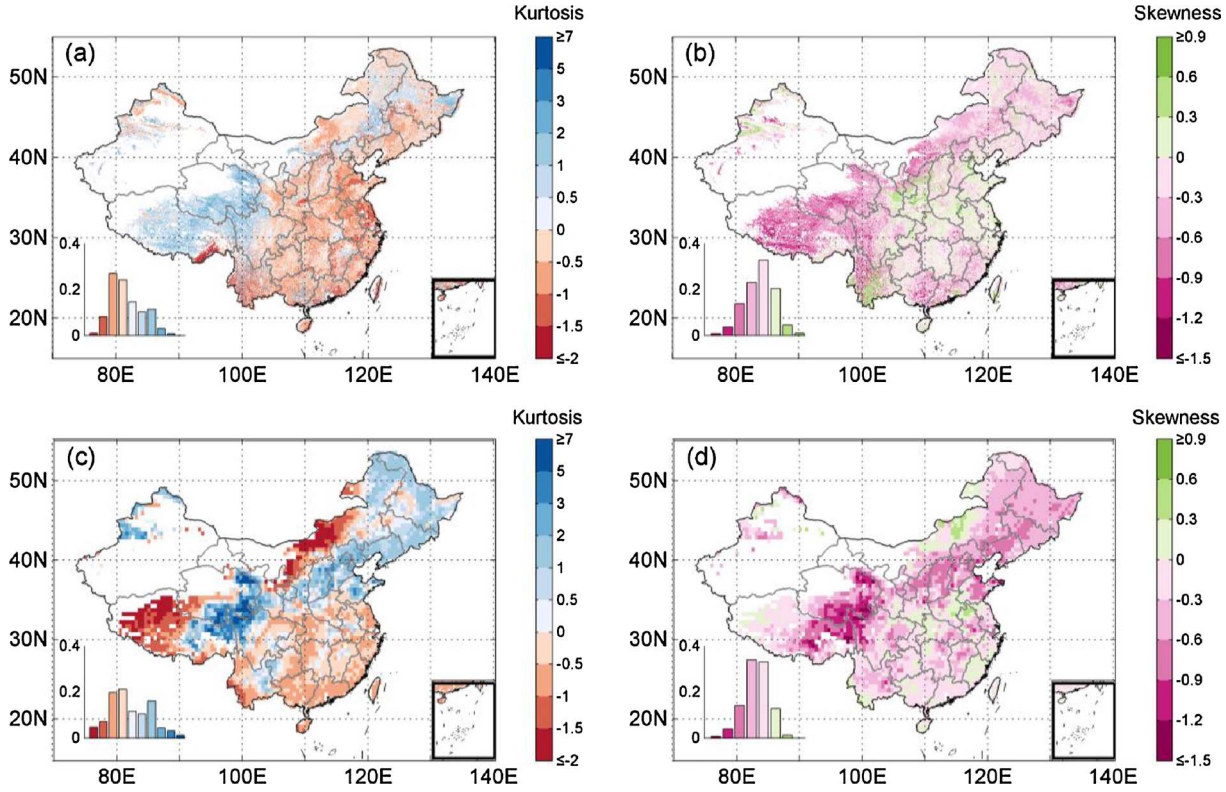

Fig. 4. The spatial distribution of (a, c) kurtosis and (b, d) skewness of seasonal NEP in China calculated for the period of 2005–2011 of (a) NEP produced in our study and (b) Jung et al. (2011).

seasonal NEP dynamics. A skewness value within ± 0.5 was deemed to be an approximately symmetrical distribution; in contrast, a negative (left-skewed) skewness indicated that the peak of the seasonal NEP was skewed to the later part of the year, and vice versa. Here, we found that the seasonal NEP dynamic in more than 70% of the areas was approximately symmetrical, except in the Tibetan Plateau and the Hengduan Mountains, where the seasonal NEP exhibited a moderately left-skewed distribution (Fig. 4b). This type of skewness for China's seasonal NEP distribution also significantly differed from the findings of Jung et al. (2011). In particular, Jung et al. (2011) identified a distinctly left-skewed seasonal NEP dynamic on the eastern edge of the Tibetan Plateau, while we found a moderately left-skewed monthly NEP distribution locally. From west to east in the Tibetan Plateau, Jung et al. (2011) derived a pronounced ascending gradient of left skewness, while a weakly opposite trend was found in our study (Fig. 4b, d). Furthermore, on the Northeast Plain and parts of North China we found roughly symmetrical seasonal C sink density distributions, rather than a gently left-skewed seasonal dynamic as in Jung et al. (2011).

3.4. Ecosystem CUE(NEP/GPP) in China

The ratio between annual NEP and annual GPP, NEP/GPP, is a direct measurement of ecosystem CUE. A higher NEP/GPP value implies higher efficiencies of photosynthate transforming into C sink. Fig. 5a shows the spatial distribution of the annual NEP/GPP ratio in China. The annual NEP/GPP ratio was larger than 0.3 over parts of Xiaoxing'anling and the Changbai Mountains in northeastern China, and in high-altitude areas such as the eastern edge of the Tibetan Plateau; the ratio was between 0.25 and 0.3 in areas bordering the southwestern and southeastern monsoon regions (Fig. 5a). These regions also had higher CUE than the rest of China (Fig. 5a). Overall, the annual NEP/GPP ratio in more than 40% of the study area fell within the range of 0.1–0.3; and the averaged ecosystem CUE was 0.17, meaning that less than 20% of the total photosynthetic products were converted into ecosystem C storage in China.

Our country average annual NEP/GPP ratio was similar to the one derived by Jung et al. (2011; 0.18). However, we found a very different spatial distribution pattern of CUE than Jung et al. (2011). CUE was

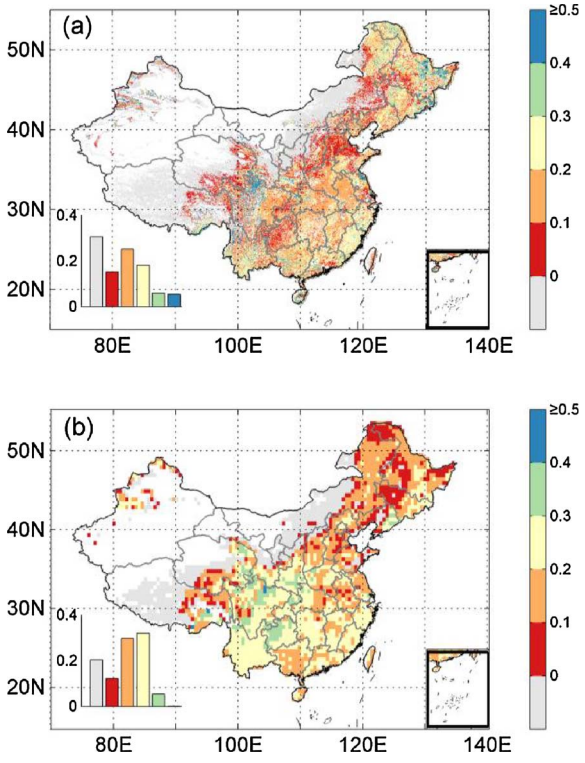

Fig. 5. The spatial pattern of the mean annual NEP/GPP ratio (a) in our study and (b) in Jung et al. (2011).

higher in our study than in Jung et al. (2011) in roughly 40% of the area examined, particularly in northeastern China where the largest inter-study discrepancy in the annual NEP/GPP ratio was about 0.2 (Fig. 5a, b). In other parts of China, predominantly in North China, the southwest monsoon regions, and central China, we derived a lower annual NEP/GPP ratio than did Jung et al. (2011) (Fig. 5a, b). In some parts of the southwestern monsoon regions, our estimated ecosystem CUE was less than Jung et al. (2011) by a unit of 0.15 (Fig. 5a, b). It is noteworthy that in areas where the two studies had large discrepancy in the estimation of annual NEP/GPP ratios, it is more likely a difference in NEP rather than GPP estimates (Fig. A.5 in the Supplementary material).

4. Discussion

Accurately characterizing the size of China's C sink is critical for understanding its role in regional and global C cycles. Previous studies based on bottom-up (national inventory and process-based models) and top-down (atmospheric inversion) approaches (Jiang et al., 2016; Piao et al., 2009b; Tian et al., 2011a, 2011b) suggested that China's terrestrial ecosystems function as C sink, sequestrating 0.18–0.35 Pg C yr^{-1}. Here, however, we found that China's terrestrial NEP during the last decade upscaled from flux observations was as large as 1.18 ± 0.05 Pg C yr^{-1}. Nonetheless, it should be noted that because NEP is the imbalance between GPP and TER, it does not account for some key component fluxes such as the lateral fluxes of non-CO_2 gaseous compound loss (e.g., volatile organic carbon [VOC], methane [CH_4], and carbon monoxide [CO]), C loss from soil erosion, harvest and grazing, and non-respiratory CO_2 losses (e.g., fire emissions) from ecosystems (Chapin et al., 2006; Jung et al., 2011; Lovett et al., 2006; Luyssaert et al., 2007; Wang and Wesche, 2016). Therefore, our flux-based NEP estimate should not be directly compared to those from bottom-up or top-down C accounting approaches from earlier studies. After accounting for other component fluxes based on published estimates (C losses of non-CO_2 gaseous compounds (including VOC, CH_4, and CO) (Piao et al., 2009b); C releases due to soil erosion (Jiang et al., 2016); agriculturally harvested biomass (National Bureau of Statistics of China, 2016); C emissions caused by non-forest fires (Song et al., 2009); land use change and management (include forest fires) C budget (Lai et al., 2016)), we estimated that China's terrestrial ecosystem functioned as C sink for 0.65 Pg C yr^{-1} over the last decade (Table 1), which is still much larger than previous estimations. This large discrepancy between current research and earlier studies (e.g., Ichii et al., 2017; Thompson et al., 2016; Tian et al., 2011a,b) is tied to the large uncertainties in those subtracted component fluxes, such as C loss from soil erosion (Jiang et al., 2016; Zhang et al., 2014).

On the other hand, our NEP estimation was close to the value estimated by Jung et al. (2011, 1.22 ± 0.06 Pg C yr^{-1}) during the same time period. Accordingly, our estimate of China's terrestrial ecosystem NEP was about 6.8% of global annual NEP (Jung et al., 2011). However, while our estimate of terrestrial NEP of the entire country agreed well with that of Jung et al. (2011), the two studies significantly differ regarding the spatial distribution of terrestrial NEP across China. For instance, by including more representative flux sites in China (46 in this study versus 9 sites in Jung et al. (2011)) and by including detailed N deposition and forest age information, we suggest that the absence of northeastern forest flux sites in Jung et al. (2011) may be inadequate to produce plausible NEP environmental gradients, which in turn has led to an underestimation in local NEP. If the 9 flux sites used in Jung et al. (2011) were denoted in the climate space, all of them are located in the climate regime with mean annual temperature below 10 °C and mean annual precipitation below 1000 mm yr^{-1} (Fig. A.6 in the Supplementary material). Extrapolation then occurs since the fluxes are predicted for the climate regimes that are not sampled by these 9 flux sites. This kind of upscaling (extrapolation) would lead to the unrealistic NEP estimation. Our comparison analysis highlights that much more flux sites, which could cover a wide range of the climate space, are needed to reduce the uncertainty in MTE upscaling of flux observations. In addition, we re-run the MTE model without using N deposition and forest age as additional explanatory variables. As shown in Fig. A.7 in the Supplementary material, the MTE model considering effects of N deposition and forest age (R^2 = 0.76, RMSE = 0.81 gC m^{-2} day^{-1}) performs better at the site level in estimating NEE than that without incorporating these effects (R^2 = 0.68, RMSE = 0.93 gC m^{-2} day^{-1}). For example, the estimated NEP without considering N deposition does not work well in cropland, since which acts as a carbon source for atmospheric CO_2 in northeastern plain and part of North China (Fig. A.8 in the Supplementary material). Annual NEP for forests in Changbai Mountains is even higher than the annual net primary productivity (NPP) (Fig. A.8 in the Supplementary material). In addition, annual NEP in north of Yunnan province is also unrealistically high (> 700 gC m^{-2} yr^{-1}), compared to our estimate considering effects of N deposition and forest age (< 500 gC m^{-2} yr^{-1}). This additional analysis highlights that including N deposition and forest age as additional explanatory variables can significantly improve NEP estimation particularly in regions with large-scale afforestation programs like southwest areas. Furthermore, different climate factor inputs could also contribute to the different spatial patterns of terrestrial NEP found in Jung et al. (2011). In particular, Jung et al. (2011) used potential radiation as an explanatory variable, which does not change over the years, rather than monthly radiation, which varies annually. A study performed in Sapporo, Japan, whose latitude is similar to that of China's northeastern forest ecosystems, found that annual NEP was closely related to shortwave radiation (Kitamura et al., 2012). Therefore, the use of seasonal potential radiation without considering its inter-annual variability in Jung et al. (2011) may also be a possible source of bias in regional C sink estimation. The difference in radiation variables may also partly explain the NEP discrepancy in some southwest China areas between our study and Jung et al. (2011), because diffuse radiation has been recognized as an important factor contributing to the large C sink of subtropical forests in southwest China (Tan et al., 2011). Furthermore, the insufficient consideration of human management activities may also contribute to the uncertainties in regional NEP estimates. For example, vegetation in the Sichuan Basin is largely dominated by croplands, whose NEP can only be indirectly estimated via vegetation proxy of FPAR in the current upscaling process, which is very uncertain (Ichii et al., 2017; Osborne et al., 2010; Smith et al., 2010). Overall, the remarkable spatial difference in terrestrial

Table 1
Synthesis of component C fluxes that are not accounted for in our NEE-based NEP estimates in China.

C balance component flux	Values (Pg C yr^{-1})	Methods	References
Fire emissions (non-forest)	0.003	Satellite	Song et al. (2009)
Land use change and land management emissions (including forest fire)[a]	0.07	Satellite and inventories	Lai et al. (2016)
Crop harvest	0.25	Inventories	National Bureau of Statistics of China (2016)
VOC, CO and CH_4	0.10	Transport model	Piao et al. (2009b)
Soil erosion	0.11	Inventories	Jiang et al. (2016)

[a] Land use management emissions include emissions from forest fires, pests and diseases, timber harvesting, firewood collection, fertilization, and drainage (Lai et al., 2016).

NEP estimates between our study and that of Jung et al. (2011) highlights the importance of incorporating more vegetation growth-related explanatory variables and more representative flux sites in NEP upscaling.

Although MTE model generally well captures the NEP at the site level, our neglect of the legacy effects of historical climate change on NEP might suggest a high risk of over-fitting. But such over-fitting issue might not be as severe as we thought. On the one hand, Yu et al. (2013) documented a strong linear relationship between GPP and NEP over all terrestrial ecosystems in China (including forest, cropland, grassland and wetland), tentatively suggesting that factors determining GPP such as meteorological variables and canopy properties could play an important role in NEP estimation. On the other hand, we have included the forest age in the MTE algorithm, which considers the effect of history disturbance regime to a certain extent. Such demographic process affects the carbon decomposition and changes in NPP during the forest succession (Amiro et al., 2010). For example, including forest age can significantly improve the MTE model performance in NEP estimation (Fig. A.7 in the Supplementary material). But these arguments may not be enough to fully justify the neglect of historical legacy effects on the carbon pool and then NEP. Further studies based on the collection of metadata and including other historical regimes as candidate predictors should be conducted.

While there still exists large uncertainties in the estimation of local- to country-level NEP and their driving variables in China, several factors could be particularly important for explaining the observed spatial pattern of China's terrestrial C sink distribution. In particular, CO_2 fertilization may be a major factor contributing to China's current net C uptake (Piao et al., 2012; Tian et al., 2011a). The rise of atmospheric CO_2 concentration stimulates vegetation growth, further enlarging net C uptake (Sitch et al., 2007). Furthermore, climate warming generally enhances C sequestration in China through extending the C sequestration period (Keenan et al., 2014; Peng et al., 2013); this warming effect, however, contributes differently to C cycles in China's northern and southern regions (Piao et al., 2012). For example, warming intensifies water limitation, and together with the decrease in rainfall over recent years, this may be a major contributor to the local C source in Inner Mongolia (Piao et al., 2010). By contrast, warming in southern China enhances the strength of local C sinks (Piao et al., 2012). In addition to the above CO_2 fertilization and climate change effects, enhanced anthropogenic N deposition in China (Liu et al., 2013) has also significantly facilitated vegetation growth, particularly in southeast China (Piao et al., 2015), and consequently the strength of C sequestration (Lu et al., 2012; Tian et al., 2011a; Yu et al., 2014). Finally, forest age is another important variable responsible for the large spatial and temporal variability in C fluxes (Amiro et al., 2010; Tang et al., 2014). The highest C sequestration capacity was found in young forest plantations less than 50 years old (Gao et al., 2016; Yu et al., 2014). And the spatial distribution of forest age is also highly heterogeneous, which favors southern China's forests in C sequestration capacity given their overly young forest structures. The effects of forest ages, however, have not been explicitly quantified in process-based models that measure China's C balance (Piao et al., 2012; Tian et al., 2011a). Because young forests less than 40 years old currently account for more than 60% of China's forested area trees (Zhang et al., 2017), future modeling studies on China's C cycle trajectory need to explicitly include forest age information. Collectively, CO_2 fertilization, climate change, high N deposition and young forest age together contribute to the large C sink in the southern China.

5. Conclusions

In this study, we empirically estimated China's land NEP at a high spatial resolution (1 km × 1 km) based on a model tree ensemble approach and used 46 flux sites located in China and its neighboring countries. By including more flux sites, as well as N deposition and forest age information, we found that China's annual land NEP over the period of 2005–2015 was 1.18 ± 0.05 Pg C yr^{-1}, a result similar to that of Jung et al. (2011). However, we found that the spatial distributions of annual NEP, seasonality, and ecosystem CUE differ greatly from those found by Jung et al. (2011). The greater number of flux sites used in our study (46 in our study versus 9 in Jung et al., 2011) may explain the improved spatial distribution estimation of China's land NEP. Nonetheless, there are still some uncertainties in our estimation. Further studies should include more flux sites in NEP upscaling. Furthermore, it should be noted that NEP is not equivalent to C sink. NEP is the difference between GPP and TER, where lateral fluxes, C loss from soil erosion, grazing and harvesting and non-respiratory CO_2 losses from ecosystems are not accounted for in the NEP estimation. To reduce the uncertainties in C sink estimation, we also need to carefully evaluate those unaccounted component fluxes. Only by doing this, will we be able to obtain a more accurate picture of the C sink strength in China and formulate climate change mitigation strategies accordingly.

Acknowledgements

This study was supported by the National Basic Research Program of China (Grant No. 2013CB956303), National Natural Science Foundation of China (41530528), and National Youth Top-notch Talent Support Program in China.

Appendix A. Supplementary data

Supplementary material related to this article can be found, in the online version, at doi:https://doi.org/10.1016/j.agrformet.2018.02.007.

References

Amiro, B.D., Barr, A.G., Barr, J.G., Black, T.A., Bracho, R., Brown, M., Chen, J., Clark, K.L., Davis, K.J., Desai, A.R., Dore, S., Engel, V., Fuentes, J.D., Goldstein, A.H., Goulden, M.L., Kolb, T.E., Lavigne, M.B., Law, B.E., Margolis, H.A., Martin, T., McCaughey, J.H., Misson, L., Montes-Helu, M., Noormets, A., Randerson, J.T., Starr, G., Xiao, J., 2010. Ecosystem carbon dioxide fluxes after disturbance in forests of North America. J. Geophys. Res. Biogeosci. 115, G00K02. http://dx.doi.org/10.1029/2010JG001390.

Anav, A., Friedlingstein, P., Kidston, M., Bopp, L., Ciais, P., Cox, P., Jones, C., Jung, M., Myneni, R.B., Zhu, Z.C., 2013. Evaluating the land and ocean components of the global carbon cycle in the CMIP5 Earth System Models. J. Clim. 26, 6801–6843.

Arnan, X., Gaucherel, C., Andersen, A.N., 2011. Dominance and species co-occurrence in highly diverse ant communities: a test of the interstitial hypothesis and discovery of a three-tiered competition cascade. Oecologia 166, 783–794.

Baldocchi, D.D., 2008. TURNER REVIEW No. 15.'Breathing'of the terrestrial biosphere: lessons learned from a global network of carbon dioxide flux measurement systems. Aust. J. Bot. 56, 1–26.

Baldocchi, D.D., 2014. Measuring fluxes of trace gases and energy between ecosystems and the atmosphere–the state and future of the eddy covariance method. Glob. Change Biol. 20, 3600–3609.

Beer, C., Reichstein, M., Tomelleri, E., Ciais, P., Jung, M., Carvalhais, N., Rödenbeck, C., Arain, M.A., Baldocchi, D., Bonan, G.B., Bondeau, A., Cescatti, A., Lasslop, G., Lindroth, A., Lomas, M., Luyssaert, S., Margolis, H., Oleson, K.W., Roupsard, O., Veenendaal, E., Viovy, N., Williams, C., Woodward, F.I., Papale, D., 2010. Terrestrial gross carbon dioxide uptake: global distribution and covariation with climate. Science 329, 834–838.

Canadell, J.G., Ciais, P., Gurney, K., Le Quéré, C., Piao, S.L., Raupach, M.R., Sabine, C.L., 2011. An international effort to quantify regional carbon fluxes. Eos Trans. AGU 92, 81–82.

Cao, M.K., Prince, S.D., Li, K.R., Tao, B., Small, J., Shao, X.M., 2003. Response of terrestrial carbon uptake to climate interannual variability in China. Glob. Change Biol. 9, 536–546.

Chapin, F.S., Woodwell, G.M., Randerson, J.T., Rastetter, E.B., Lovett, G.M., Baldocchi, D.D., Clark, D.A., Harmon, M.E., Schimel, D.S., Valentini, R., Wirth, C., Aber, J.D., Cole, J.J., Goulden, M.L., Harden, J.W., Heimann, M., Howarth, R.W., Matson, P.A., McGuire, A.D., Melillo, J.M., Mooney, H.A., Neff, J.C., Houghton, R.A., Place, M.L., Ryan, M.G., Running, S.W., Sala, O.E., Schlesinger, W.H., Schulze, E.-D., 2006. Reconciling carbon-cycle concepts, terminology, and methods. Ecosystems 9, 1041–1050.

Chen, Y.Y., Yang, K., He, J., Qin, J., Shi, J.C., Du, J.Y., He, Q., 2011. Improving land surface temperature modeling for dry land of China. J. Geophys. Res. Atmos. 116, D20104. http://dx.doi.org/10.1029/2011JD015921.

De Vries, W., Solberg, S., Dobbertin, M., Sterba, H., Laubhann, D., Van Oijen, M., Evans,

C., Gundersen, P., Kros, J., Wamelink, G., Reinds, G.J., Sutton, M.A., 2009. The impact of nitrogen deposition on carbon sequestration by European forests and heathlands. For. Ecol. Manage. 258, 1814–1823.
Denning, A.S., Randall, D.A., Collatz, G.J., Sellers, P.J., 1996. Simulations of terrestrial carbon metabolism and atmospheric CO2 in a general circulation model. Tellus B 48, 543–567.
Dentener, F., 2006. Global Maps of Atmospheric Nitrogen Deposition, 1860, 1993, and 2050. Data set. Available on-line (http://daac.ornl.gov/) from Oak Ridge National Laboratory Distributed Active Archive Center, Oak Ridge, TN, USA.
Editorial Board of Vegetation Map of China, 2007. Chinese Academy of Sciences. Vegetation Map of the People's Republic of China (1:1000000) (Digital Version). Geology Press, Beijing, China.
Fang, J.Y., Guo, Z.D., Piao, S.L., Chen, A.P., 2007. Terrestrial vegetation carbon sinks in China, 1981–2000. Sci. China Ser. D Earth Sci. 50, 1341–1350.
Fernández-Martínez, M., Vicca, S., Janssens, I.A., Sardans, J., Luyssaert, S., Campioli, M., Chapin, F.S., Ciais, P., Malhi, Y., Obersteiner, M., Papale, D., Piao, S.L., Reichstein, M., Roda, F., Penuelas, J., 2014. Nutrient availability as the key regulator of global forest carbon balance. Nat. Clim. Change 4, 471–476.
Friedlingstein, P., Cox, P., Betts, R., Bopp, L., Von Bloh, W., Brovkin, V., Cadule, P., Doney, S., Eby, M., Fung, I., Bala, G., John, J., Jones, C., Joos, F., Kato, T., Kawamiya, M., Knorr, W., Lindsay, K., Matthews, H.D., Raddatz, T., Rayner, P., Reick, C., Roeckner, E., Schnitzler, K.-G., Schnur, R., Strassmann, K., Weaver, A.J., Yoshikawa, C., Zeng, N., 2006. Climate-carbon cycle feedback analysis: Results from the C4MIP model intercomparison. J. Clim. 19, 3337–3353.
Friedlingstein, P., Meinshausen, M., Arora, V.K., Jones, C.D., Anav, A., Liddicoat, S.K., Knutti, R., 2014. Uncertainties in CMIP5 climate projections due to carbon cycle feedbacks. J. Clim. 27, 511–526.
Gao, S., Zhou, T., Zhao, X., Wu, D.H., Li, Z., Wu, H., Du, L., Luo, H., 2016. Age and climate contribution to observed forest carbon sinks in East Asia. Environ. Res. Lett. 11, 034021. http://dx.doi.org/10.1088/1748-9326/11/3/034021.
Gaucherel, C., Alleaume, S., Hely, C., 2008. The comparison map profile method: A strategy for multiscale comparison of quantitative and qualitative images. IEEE Trans. Geosci. Remote. Sens. 46, 2708–2719.
Gaucherel, C., Balasubramanian, M., Karunakaran, P., Ramesh, B., Muthusankar, G., Hély, C., Couteron, P., 2010. At which scales does landscape structure influence the spatial distribution of elephants in the Western Ghats (India)? J. Zool. 280, 185–194.
Goulden, M.L., McMillan, A.M.S., Winston, G.C., Rocha, A.V., Manies, K.L., Harden, J.W., Bond-Lamberty, B.P., 2011. Patterns of NPP, GPP, respiration, and NEP during boreal forest succession. Glob. Change Biol. 17, 855–871.
Gregory, J.M., Jones, C., Cadule, P., Friedlingstein, P., 2009. Quantifying carbon cycle feedbacks. J. Clim. 22, 5232–5250.
Gritti, E.S., Gaucherel, C., Crespo-Perez, M.V., Chuine, I., 2013. How can model comparison help improving species distribution models? PLoS ONE 8, e68823. http://dx.doi.org/10.1371/journal.pone.0068823.
Gurney, K.R., Eckels, W.J., 2011. Regional trends in terrestrial carbon exchange and their seasonal signatures. Tellus B 63, 328–339.
Holben, B.N., 1986. Characteristics of maximum-value composite images from temporal AVHRR data. Int. J. Remote Sens. 7, 1417–1434.
Huffman, G.J., Bolvin, D.T., Nelkin, E.J., Wolff, D.B., Adler, R.F., Gu, G.J., Hong, Y., Bowman, K.P., Stocker, E.F., 2007. The TRMM multisatellite precipitation analysis (TMPA): Quasi-global, multiyear, combined-sensor precipitation estimates at fine scales. J. Hydrometeorol. 8, 38–55.
Hyvönen, R., Ågren, G.I., Linder, S., Persson, T., Cotrufo, M.F., Ekblad, A., Freeman, M., Grelle, A., Janssens, I.A., Jarvis, P.G., Kellomaki, S., Lindroth, A., Loustau, D., Lundmark, T., Norby, R.J., Oren, R., Pilegaard, K., Ryan, M.G., Sigurdsson, B.D., Stromgren, M., van Oijen, M., Wallin, G., 2007. The likely impact of elevated [CO2], nitrogen deposition, increased temperature and management on carbon sequestration in temperate and boreal forest ecosystems: a literature review. New Phytol. 173, 463–480.
Ichii, K., Ueyama, M., Kondo, M., Saigusa, N., Kim, J., Alberto, M., Ardö, J., Euskirchen, E.S., Kang, M., Hirano, T., Joiner, J., Kobayashi, H., Marchesini, L.B., Merbold, L., Miyata, A., Saitoh, T.M., Takagi, K., Varlagin, A., Bret-Harte, M.S., Kitamura, K., Kosugi, Y., Kotani, A., Kumar, K., Li, S.G., Machimura, T., Matsuura, Y., Mizoguchi, Y., Ohta, T., Mukherjee, S., Yanagi, Y., Yasuda, Y., Zhang, Y.P., Zhao, F.H., 2017. New data-driven estimation of terrestrial CO2 fluxes in Asia using a standardized database of eddy covariance measurements, remote sensing data, and support vector regression. J. Geophys. Res. Biogeosci. 122, 767–795.
IPCC, 2013. Climate Change 2013: The Physical Science Basis. Contribution of Working Group I to the Fifth Assessment Report of the Intergovernmental Panel on Climate Change. IPCC, Cambridge, United Kingdom and New York, NY, USA.
Jiang, F., Chen, J.M., Zhou, L.X., Ju, W.M., Zhang, H.F., Machida, T., Ciais, P., Peters, W., Wang, H.M., Chen, B.Z., Liu, L.X., Zhang, C.H., Matsueda, H., Sawa, Y., 2016. A comprehensive estimate of recent carbon sinks in China using both top-down and bottom-up approaches. Sci. Rep. 6, 22130. http://dx.doi.org/10.1038/srep22130.
Jung, M., Reichstein, M., Bondeau, A., 2009. Towards global empirical upscaling of FLUXNET eddy covariance observations: validation of a model tree ensemble approach using a biosphere model. Biogeoscience 6, 2001–2013.
Jung, M., Reichstein, M., Ciais, P., Seneviratne, S.I., Sheffield, J., Goulden, M.L., Bonan, G., Cescatti, A., Chen, J.Q., De Jeu, R., Dolman, A.J., Eugster, W., Gerten, D., Gianelle, D., Gobron, N., Heinke, J., Kimball, J., Law, B.E., Montagnani, L., Mu, Q.Z., Mueller, B., Oleson, K., Papale, D., Richardson, A.D., Roupsard, O., Running, S., Tomelleri, E., Viovy, N., Weber, U., Williams, C., Wood, E., Zaehle, S., Zhang, K., 2010. Recent decline in the global land evapotranspiration trend due to limited moisture supply. Nature 467, 951–954.
Jung, M., Reichstein, M., Margolis, H.A., Cescatti, A., Richardson, A.D., Arain, M.A., Arneth, A., Bernhofer, C., Bonal, D., Chen, J.Q., Gianelle, D., Gobron, N., Kiely, G., Kutsch, W., Lasslop, G., Law, B.E., Lindroth, A., Merbold, L., Montagnani, L., Moors, E.J., Papale, D., Sottocornola, M., Vaccari, F., Williams, C., 2011. Global patterns of land-atmosphere fluxes of carbon dioxide, latent heat, and sensible heat derived from eddy covariance, satellite, and meteorological observations. J. Geophys. Res. Biogeosci. 116, G00J07. http://dx.doi.org/10.1029/2010JG001566.
Keenan, T.F., Gray, J., Friedl, M.A., Toomey, M., Bohrer, G., Hollinger, D.Y., Munger, J.W., O'Keefe, J., Schmid, H.P., Wing, I.S., Yang, B., Richardson, A.D., 2014. Net carbon uptake has increased through warming-induced changes in temperate forest phenology. Nat. Clim. Change 4, 598–604.
Kitamura, K., Nakai, Y., Suzuki, S., Ohtani, Y., Yamanoi, K., Sakamoto, T., 2012. Interannual variability of net ecosystem production for a broadleaf deciduous forest in Sapporo, northern Japan. J. For. Res. 17, 323–332.
Krinner, G., Viovy, N., de Noblet-Ducoudré, N., Ogée, J., Polcher, J., Friedlingstein, P., Ciais, P., Sitch, S., Prentice, I.C., 2005. A dynamic global vegetation model for studies of the coupled atmosphere-biosphere system. Glob. Biogeochem. Cycles 19, GB1015. http://dx.doi.org/10.1029/2003GB002199.
Lai, L., Huang, X.J., Yang, H., Chuai, X.W., Zhang, M., Zhong, T.Y., Chen, Z.G., Chen, Y., Wang, X., Thompson, J.R., 2016. Carbon emissions from land-use change and management in China between 1990 and 2010. Sci. Adv. 2, e1601063. http://dx.doi.org/10.1126/sciadv.1601063.
Le Quéré, C., Moriarty, R., Andrew, R.M., Canadell, J.G., Sitch, S., Korsbakken, J.I., Friedlingstein, P., Peters, G.P., Andres, R.J., Boden, T.A., Houghton, R.A., House, J.I., Keeling, R.F., Tans, P., Arneth, A., Bakker, D.C.E., Barbero, L., Bopp, L., Chang, J., Chevallier, F., Chini, L.P., Ciais, P., Fader, M., Feely, R.A., Gkritzalis, T., Harris, I., Hauck, J., Ilyina, T., Jain, A.K., Kato, E., Kitidis, V., Klein Goldewijk, K., Koven, C., Landschützer, P., Lauvset, S.K., Lefèvre, N., Lenton, A., Lima, I.D., Metzl, N., Millero, F., Munro, D.R., Murata, A., Nabel, J.E.M.S., Nakaoka, S., Nojiri, Y., O'Brien, K., Olsen, A., Ono, T., Pérez, F.F., Pfeil, B., Pierrot, D., Poulter, B., Rehder, G., Rödenbeck, C., Saito, S., Schuster, U., Schwinger, J., Séférian, R., Steinhoff, T., Stocker, B.D., Sutton, A.J., Takahashi, T., Tilbrook, B., van der Laan-Luijkx, I.T., van der Werf, G.R., van Heuven, S., Vandemark, D., Viovy, N., Wiltshire, A., Zaehle, S., Zeng, N., 2015. Global carbon budget 2015. Earth Syst. Sci. Data 7, 349–396. http://dx.doi.org/10.5194/essd-7-349-2015.
Le Quéré, C., Raupach, M.R., Canadell, J.G., Marland, G., Bopp, L., Ciais, P., Conway, T.J., Doney, S.C., Feely, R.A., Foster, P., Friedlingstein, P., Gurney, K., Houghton, R.A., House, J.I., Huntingford, C., Levy, P.E., Lomas, M.R., Majkut, J., Metzl, N., Ometto, J.P., Peters, G.P., Prentice, I.C., Randerson, J.T., Running, S.W., Sarmiento, J.L., Schuster, U., Sitch, S., Takahashi, T., Viovy, N., van der Werf, G.R., Woodward, F.I., 2009. Trends in the sources and sinks of carbon dioxide. Nat. Geosci. 2, 831–836.
Liu, X.J., Zhang, Y., Han, W.X., Tang, A.H., Shen, J.L., Cui, Z.L., Vitousek, P., Erisman, J.W., Goulding, K., Christie, P., Fangmeier, A., Zhang, F.S., 2013. Enhanced nitrogen deposition over China. Nature 494, 459–462.
Lovett, G.M., Cole, J.J., Pace, M.L., 2006. Is net ecosystem production equal to ecosystem carbon accumulation? Ecosystems 9, 152–155.
Lu, C.Q., Tian, H.Q., Liu, M.L., Ren, W., Xu, X.F., Chen, G.S., Zhang, C., 2012. Effect of nitrogen deposition on China's terrestrial carbon uptake in the context of multifactor environmental changes. Ecol. Appl. 22, 53–75.
Luyssaert, S., Inglima, I., Jung, M., Richardson, A.D., Reichstein, M., Papale, D., Piao, S.L., Schulze, E.D., Wingate, L., Matteucci, G., Aragao, L., Aubinet, M., Beer, C., Bernhofer, C., Black, K.G., Bonal, D., Bonnefond, J.M., Chambers, J., Ciais, P., Cook, B., Davis, K.J., Dolman, A.J., Gielen, B., Goulden, M., Grace, J., Granier, A., Grelle, A., Griffis, T., Grünwald, T., Guidolotti, G., Hanson, P.J., Harding, R., Hollinger, D.Y., Hutyra, L.R., Kolari, P., Kruijt, B., Kutsch, W., Lagergren, F., Laurila, T., Law, B.E., Le Mair, G., Lindroth, A., Loustau, D., Malhi, Y., Mateus, J., Migliavacca, M., Misson, L., Montagnani, L., Moncrieff, J., Moors, E., Munger, J.W., Nikinmaa, E., Ollinger, S.V., Pita, G., Rebmann, C., Roupsard, O., Saigusa, N., Sanz, M.J., Seufert, G., Sierra, C., Smith, M.L., Tang, J., Valentini, R., Vesala, T., Janssens, I.A., 2007. CO2 balance of boreal, temperate, and tropical forests derived from a global database. Glob. Change Biol. 13, 2509–2537.
Luyssaert, S., Schulze, E.D., Börner, A., Knohl, A., Hessenmöller, D., Law, B.E., Ciais, P., Grace, J., 2008. Old-growth forests as global carbon sinks. Nature 455, 213–215.
Magnani, F., Mencuccini, M., Borghetti, M., Berbigier, P., Berninger, F., Delzon, S., Grelle, A., Hari, P., Jarvis, P.G., Kolari, P., Kowalski, A.S., Lankreijer, H., Law, B.E., Lindroth, A., Loustau, D., Manca, G., Moncrieff, J.B., Rayment, M., Tedeschi, V., Valentini, R., Grace, J., 2007. The human footprint in the carbon cycle of temperate and boreal forests. Nature 447, 848–850.
Myneni, R.B., Hoffman, S., Knyazikhin, Y., Privette, J.L., Glassy, J., Tian, Y., Wang, Y., Song, X., Zhang, Y., Smith, G.R., Lotsch, A., Friedl, M., Morisette, J.T., Votava, P., Nemani, R.R., Running, S.W., 2002. Global products of vegetation leaf area and fraction absorbed PAR from year one of MODIS data. Remote Sens. Environ. 83, 214–231.
National Bureau of Statistics of China, 2016. China Statistical Year Book. China Statistical Press, Beijing.
Osborne, B., Saunders, M., Walmsley, D., Jones, M., Smith, P., 2010. Key questions and uncertainties associated with the assessment of the cropland greenhouse gas balance. Agric. Ecosyst. Environ. 139, 293–301.
Pacala, S.W., Hurtt, G.C., Baker, D., Peylin, P., Houghton, R.A., Birdsey, R.A., Heath, L., Sundquist, E.T., Stallard, R.F., Ciais, P., Moorcroft, P., Caspersen, J.P., Shevliakova, E., Moore, B., Kohlmaier, G., Holland, E., Gloor, M., Harmon, M.E., Fan, S.M., Sarmiento, J.L., Goodale, C.L., Schimel, D., Field, C.B., 2001. Consistent land- and atmosphere-based US carbon sink estimates. Science 292, 2316–2320.
Pan, Y.D., Birdsey, R.A., Fang, J., Houghton, R., Kauppi, P.E., Kurz, W.A., Phillips, O.L., Shvidenko, A., Lewis, S.L., Canadell, J.G., Ciais, P., Jackson, R.B., Pacala, S.W., McGuire, A.D., Piao, S.L., Rautiainen, A., Sitch, S., Hayes, D., 2011. A large and persistent carbon sink in the world's forests. Science 333, 988–993.
Peng, S.S., Piao, S.L., Ciais, P., Myneni, R.B., Chen, A.P., Chevallier, F., Dolman, A.J.,

Janssens, I.A., Penuelas, J., Zhang, G.X., Vicca, S., Wan, S.Q., Wang, S.P., Zeng, H., 2013. Asymmetric effects of daytime and night-time warming on Northern Hemisphere vegetation. Nature 501, 88–92.

Piao, S.L., Ciais, P., Friedlingstein, P., de Noblet-Ducoudré, N., Cadule, P., Viovy, N., Wang, T., 2009a. Spatiotemporal patterns of terrestrial carbon cycle during the 20th century. Glob. Biogeochem. Cycles 23, GB4026. http://dx.doi.org/10.1029/2008GB003339.

Piao, S.L., Ciais, P., Huang, Y., Shen, Z.H., Peng, S.S., Li, J.S., Zhou, L.P., Liu, H.Y., Ma, Y.C., Ding, Y.H., Friedlingstein, P., Liu, C.Z., Tan, K., Yu, Y.Q., Zhang, T.Y., Fang, J.Y., 2010. The impacts of climate change on water resources and agriculture in China. Nature 467, 43–51.

Piao, S.L., Fang, J.Y., Ciais, P., Peylin, P., Huang, Y., Sitch, S., Wang, T., 2009b. The carbon balance of terrestrial ecosystems in China. Nature 458, 1009–1013.

Piao, S.L., Ito, A., Li, S.G., Huang, Y., Ciais, P., Wang, X.H., Peng, S.S., Nan, H.J., Zhao, C., Ahlström, A., Andres, R.J., Chevallier, F., Fang, J., Hartmann, J., Huntingford, C., Jeong, S., Levis, S., Levy, P.E., Li, J.S., Lomas, M.R., Mao, J.F., Mayorga, E., Mohammat, A., Muraoka, H., Peng, C.H., Peylin, P., Poulter, B., Shen, Z.H., Shi, X., Sitch, S., Tao, S., Tian, H.Q., Wu, X.P., Xu, M., Yu, G.R., Viovy, N., Zaehle, S., Zeng, N., Zhu, B., 2012. The carbon budget of terrestrial ecosystems in East Asia over the last two decades. Biogeoscience 9, 3571–3586.

Piao, S.L., Sitch, S., Ciais, P., Friedlingstein, P., Peylin, P., Wang, X.H., Ahlström, A., Anav, A., Canadell, J.G., Cong, N., Huntingford, C., Jung, M., Levis, S., Levy, P.E., Li, J.S., Lin, X., Lomas, M.R., Lu, M., Luo, Y.Q., Ma, Y.C., Myneni, R.B., Poulter, B., Sun, Z.Z., Wang, T., Viovy, N., Zaehle, S., Zeng, N., 2013. Evaluation of terrestrial carbon cycle models for their response to climate variability and to CO2 trends. Glob. Change Biol. 19, 2117–2132.

Piao, S.L., Yin, G.D., Tan, J.G., Cheng, L., Huang, M.T., Li, Y., Liu, R.G., Mao, J.F., Myneni, R.B., Peng, S.S., Poulter, B., Shi, X.Y., Xiao, Z.Q., Zeng, N., Zeng, Z.Z., Wang, Y.P., 2015. Detection and attribution of vegetation greening trend in China over the last 30 years. Glob. Change Biol. 21, 1601–1609.

Pregitzer, K.S., Euskirchen, E.S., 2004. Carbon cycling and storage in world forests: biome patterns related to forest age. Glob. Change Biol. 10, 2052–2077.

Saigusa, N., Li, S.G., Kwon, H., Takagi, K., Zhang, L.M., Ide, R., Ueyama, M., Asanuma, J., Choi, Y.J., Chun, J.H., Han, S.J., Hirano, T., Hirata, R., Kang, M., Kato, T., Kim, J., Li, Y.N., Maeda, T., Miyata, A., Mizoguchi, Y., Murayama, S., Nakai, Y., Ohta, T., Saitoh, T.M., Wang, H.M., Yu, G.R., Zhang, Y.P., Zhao, F.H., 2013. Dataset of CarboEastAsia and uncertainties in the CO2 budget evaluation caused by different data processing. J. For. Res. 18, 41–48.

Schwalm, C.R., Williams, C.A., Schaefer, K., Baldocchi, D.D., Black, T.A., Goldstein, A.H., Law, B.E., Oechel, W., Scott, R.L., 2012. Reduction in carbon uptake during turn of the century drought in western North America. Nat. Geosci. 5, 551–556.

Sheffield, J., Goteti, G., Wood, E.F., 2006. Development of a 50-year high-resolution global dataset of meteorological forcings for land surface modeling. J. Clim. 19, 3088–3111.

Sitch, S., Cox, P., Collins, W., Huntingford, C., 2007. Indirect radiative forcing of climate change through ozone effects on the land-carbon sink. Nature 448, 791–794.

Sitch, S., Smith, B., Prentice, I.C., Arneth, A., Bondeau, A., Cramer, W., Kaplan, J., Levis, S., Lucht, W., Sykes, M.T., Thonicke, K., Venevsky, S., 2003. Evaluation of ecosystem dynamics, plant geography and terrestrial carbon cycling in the LPJ dynamic global vegetation model. Glob. Change Biol. 9, 161–185.

Smith, P., Lanigan, G., Kutsch, W.L., Buchmann, N., Eugster, W., Aubinet, M., Ceschia, E., Béziat, P., Yeluripati, J.B., Osborne, B., Moors, E.J., Brut, A., Wattenbach, M., Saunders, M., Jones, M., 2010. Measurements necessary for assessing the net ecosystem carbon budget of croplands. Agric. Ecosyst. Environ. 139, 302–315.

Song, Y., Liu, B., Miao, W.J., Chang, D., Zhang, Y.H., 2009. Spatiotemporal variation in nonagricultural open fire emissions in China from 2000 to 2007. Glob. Biogeochem. Cycles 23, GB2008. http://dx.doi.org/10.1029/2008GB003344.

Sutton, M.A., Simpson, D., Levy, P.E., Smith, R.I., Reis, S., Van Oijen, M., De Vries, W., 2008. Uncertainties in the relationship between atmospheric nitrogen deposition and forest carbon sequestration. Glob. Change Biol. 14, 2057–2063.

Tan, Z.H., Zhang, Y.P., Schaefer, D., Yu, G.R., Liang, N.S., Song, Q.H., 2011. An old-growth subtropical Asian evergreen forest as a large carbon sink. Atmos. Environ. 45, 1548–1554.

Tang, J.W., Luyssaert, S., Richardson, A.D., Kutsch, W., Janssens, I.A., 2014. Steeper declines in forest photosynthesis than respiration explain age-driven decreases in forest growth. Proc. Natl. Acad. Sci. U. S. A. 111, 8856–8860.

Tans, P.P., Fung, I.Y., Takahashi, T., 1990. Observational constraints on the global atmospheric CO2 budget. Science 247, 1431–1438.

Thompson, R.L., Patra, P.K., Chevallier, F., Maksyutov, S., Law, R.M., Ziehn, T., Van der Laan-luijkx, I.T., Peters, W., Ganshin, A., Zhuravlev, R., Maki, T., Nakamura, T., Shirai, T., Ishizawa, M., Saeki, T., Machida, T., Poulter, B., Canadell, J.G., Ciais, P., 2016. Top-down assessment of the Asian carbon budget since the mid 1990s. Nat. Commun. 7, 10724. http://dx.doi.org/10.1038/ncomms10724.

Tian, H.Q., Melillo, J., Lu, C.Q., Kicklighter, D., Liu, M.L., Ren, W., Xu, X.F., Chen, G.S., Zhang, C., Pan, S.F., Liu, J.Y., Running, S., 2011a. China's terrestrial carbon balance: contributions from multiple global change factors. Glob. Biogeochem. Cycles 25, GB1007. http://dx.doi.org/10.1029/2010GB003838.

Tian, H.Q., Xu, X.F., Liu, M.L., Ren, W., Zhang, C., Chen, G.S., Lu, C.Q., 2010. Spatial and temporal patterns of CH4 and N2O fluxes in terrestrial ecosystems of North America during 1979–2008: application of a global biogeochemistry model. Biogeoscience 7, 2673–2694.

Tian, H.Q., Xu, X.F., Lu, C.Q., Liu, M.L., Ren, W., Chen, G.S., Melillo, J., Liu, J.Y., 2011b. Net exchanges of CO2, CH4, and N2O between China's terrestrial ecosystems and the atmosphere and their contributions to global climate warming. J. Geophys. Res. Biogeosci. 116, G02011. http://dx.doi.org/10.1029/2010JG001393.

Wang, X.H., Piao, S.L., Ciais, P., Friedlingstein, P., Myneni, R.B., Cox, P., Heimann, M., Miller, J., Peng, S.S., Wang, T., Yang, H., Chen, A.P., 2014. A two-fold increase of carbon cycle sensitivity to tropical temperature variations. Nature 506, 212–215.

Wang, Y., Wesche, K., 2016. Vegetation and soil responses to livestock grazing in Central Asian grasslands: a review of Chinese literature. Biodivers. Conserv. 25, 2401–2420.

Wei, Y.X., Liu, S.S., Huntzinger, D.N., Michalak, A.M., Viovy, N., Post, W.M., Schwalm, C.R., Schaefer, K., Jacobson, A.R., Lu, C.Q., Tian, H.Q., Ricciuto, D.M., Cook, R.B., Mao, J.F., Shi, X.Y., 2014. The North American carbon program multi-scale synthesis and terrestrial model intercomparison project–Part 2: environmental driver data. Geosci. Model Dev. 7, 2875–2893.

Xiao, J.F., Davis, K.J., Urban, N.M., Keller, K., Saliendra, N.Z., 2011a. Upscaling carbon fluxes from towers to the regional scale: Influence of parameter variability and land cover representation on regional flux estimates. J. Geophys. Res. Biogeosci. 116, G00J06. http://dx.doi.org/10.1029/2010JG001568.

Xiao, J.F., Zhuang, Q.L., Baldocchi, D.D., Law, B.E., Richardson, A.D., Chen, J.Q., Oren, R., Starr, G., Noormets, A., Ma, S.Y., Verma, S.B., Wharton, S., Wofsy, S.C., Bolstad, P.V., Burns, S.P., Cook, D.R., Curtis, P.S., Drake, B.G., Falk, M., Fischer, M.L., Foster, D.R., Gu, L.H., Hadley, J.L., Hollinger, D.Y., Katul, G.G., Litvak, M., Martin, T.A., Matamala, R., McNulty, S., Meyers, T.P., Monson, R.K., Munger, J.W., Oechel, W.C., Paw U, K.T., Schmid, H.P., Scott, R.L., Sun, G., Suyker, A.E., Torn, M.S., 2008. Estimationofnet ecosystemcarbonexchange for the conterminous United States by combining MODIS and AmeriFlux data. Agric. For. Meteorol. 148, 1827–1847.

Xiao, J.F., Zhuang, Q.L., Law, B.E., Baldocchi, D.D., Chen, J.Q., Richardson, A.D., Melillo, J.M., Davis, K.J., Hollinger, D.Y., Wharton, S., Oren, R., Noormets, A., Fischer, M.L., Verma, S.B., Cook, D.R., Sun, G., McNulty, S., Wofsy, S.C., Bolstad, P.V., Burns, S.P., Curtis, P.S., Drake, B.G., Falk, M., Foster, D.R., Gu, L.H., Hadley, J.L., Katulk, G.G., Litvak, M., Ma, S.Y., Martinz, T.A., Matamala, R., Meyers, T.P., Monson, R.K., Munger, J.W., Oechel, W.C., Paw U, K.T., Schmid, H.P., Scott, R.L., Starr, G., Suyker, A.E., Torn, M.S., 2011b. Assessing net ecosystem carbon exchange of US terrestrial ecosystems by integrating eddy covariance flux measurements and satellite observations. Agric. For. Meteorol. 151, 60–69.

Yang, K., He, J., Tang, W.J., Qin, J., Cheng, C.C., 2010. On downward shortwave and longwave radiations over high altitude regions: Observation and modeling in the Tibetan Plateau. Agric. For. Meteorol. 150, 38–46.

Yang, K., Koike, T., Ye, B.S., 2006. Improving estimation of hourly, daily, and monthly solar radiation by importing global data sets. Agric. For. Meteorol. 137, 43–55.

Yao, Y., Wang, X., Li, Y., Wang, T., Shen, M., Du, M., He, H., Li, Y., Luo, W., Ma, M., Ma, Y., Tang, Y., Wang, H., Zhang, X., Zhang, Y., Zhao, L., Zhou, G., Piao, S., 2018. Spatiotemporal pattern of gross primary productivity and its covariation with climate in China over the last thirty years. Glob. Change Biol. 24, 184–196.

Yatagai, A., Arakawa, O., Kamiguchi, K., Kawamoto, H., Nodzu, M.I., Hamada, A., 2009. A 44-year daily gridded precipitation dataset for Asia based on a dense network of rain gauges. Sola 5, 2009–2035.

Yu, G.R., Chen, Z., Piao, S.L., Peng, C.H., Ciais, P., Wang, Q.F., Li, X.R., Zhu, X.J., 2014. High carbon dioxide uptake by subtropical forest ecosystems in the East Asian monsoon region. Proc. Natl. Acad. Sci. U. S. A. 111, 4910–4915.

Yu, G.R., Fu, Y.L., Sun, X.M., Wen, X.F., Zhang, L.M., 2006a. Recent progress and future directions of ChinaFLUX. Sci. China Ser. D Earth Sci. 49, 1–23.

Yu, G.R., Ren, W., Chen, Z., Zhang, L.M., Wang, Q.F., Wen, X.F., He, N.P., Zhang, L., Fang, H.J., Zhu, X.J., Gao, Y., Sun, X.M., 2016. Construction and progress of Chinese terrestrial ecosystem carbon, nitrogen and water fluxes coordinated observation. J. Geog. Sci. 26, 803–826.

Yu, G.R., Wen, X.F., Sun, X.M., Tanner, B.D., Lee, X., Chen, J.Y., 2006b. Overview of ChinaFLUX and evaluation of its eddy covariance measurement. Agric. For. Meteorol. 137, 125–137.

Yu, G.R., Zhu, X.J., Fu, Y.L., He, H.L., Wang, Q.F., Wen, X.F., Li, X.R., Zhang, L.M., Zhang, L., Su, W., Li, S.G., Sun, X.-M., Zhang, Y.P., Zhang, J.H., Yan, J.H., Wang, H.M., Zhou, G.S., Jia, B.R., Xiang, W.H., Li, Y.N., Zhao, L., Wang, Y.F., Shi, P.L., Chen, S.P., Xin, X.P., Zhao, F.H., Wang, Y.Y., Tong, C.L., 2013. Spatial patterns and climate drivers of carbon fluxes in terrestrial ecosystems of China. Glob. Change Biol. 19, 798–810.

Zeng, Z.Z., Wang, T., Zhou, F., Ciais, P., Mao, J.F., Shi, X.Y., Piao, S.L., 2014. A worldwide analysis of spatiotemporal changes in water balance-based evapotranspiration from 1982 to 2009. J. Geophys. Res. Atmos. 119, 1186–1202.

Zhang, H.C., Liu, S.G., Yuan, W.P., Dong, W.J., Ye, A.Z., Xie, X.H., Chen, Y., Liu, D., Cai, W.W., Mao, Y.N., 2014. Inclusion of soil carbon lateral movement alters terrestrial carbon budget in China. Sci. Rep. 4, 7247. http://dx.doi.org/10.1038/srep07247.

Zhang, Y., Yao, Y.T., Wang, X.H., Liu, Y.W., Piao, S.L., 2017. Mapping spatial distribution of forest age in China. Earth Space Sci. 4, 108–116.